THE DESIGN OF ROTOR POSITION OBSERVER FOR DFIG DURING TRANSIENT GRID VOLTAGE IMBALANCE

Qianqiong WU[1], Xiaoying CHANG[2], Meihua ZHAO[3], Mingwei LI[4]

A rotor position observer based on hysteresis comparator (HC) was presented to acquire the rotor position angle of the Doubly-fed induction generator (DFIG) under unbalanced grid Voltage conditions. The position and velocity of DFIG's rotor were estimated by the observer with hysteresis comparator. The system structure is relatively simple, without adjusting any parameters, easy to achieve. Simulation model for wind energy generation system-with DFIG is set up. The simulation results show that the control strategy is feasible and efficient.

Keywords: doubly-fed induction generator; unbalanced grid voltage, hysteresis controller, rotor position observer

1. Introduction

Doubly fed induction generator (DFIG) has been widely used in wind power system because it can realize variable speed constant frequency operation. In this system, the DFIG's stator is directly connected to the power grid, and its rotor is controlled by a dual PWM converter to realize the decoupling control of DFIG's output active and reactive power.

The position Angle (θ_r) of DFIG's rotor is a very important parameter in the study of DFIG's control strategies. It could be obtained by speed sensor [1-8] or by control technology without speed sensor (sensorless) [9-10]. Because speed sensor is not needed in sensorless control technology, so it has low cost and high reliability. It is suitable to work in bad environment. Therefore, the application of sensorless control in doubly fed wind power generation has been attracted more and more attention from scholars at home and abroad. Model Reference Adaptive System (MRAS) rotor position observer based on rotor current was proposed in

[1] Lect., College of electrical engineering and automation, Luoyang Institute of Science and Technology, Luoyang, China. State Key Laboratory of Mathematical Engineering and Advanced Computing, Zhengzhou, China, e-mail: 40913436@qq.com
[2] Lect., College of electrical engineering and automation, Luoyang Institute of Science and Technology, Luoyang, China, e-mail: xy-cp@163.com
[3] Assoc. Prof., College of electrical engineering and automation, Luoyang Institute of Science and Technology, Luoyang, China, e-mail: zhaomh2013@126.com
[4] Prof., College of electrical engineering and automation, Luoyang Institute of Science and Technology, Luoyang, China, e-mail: lmw7301@163.com

Literature [11], the estimation accuracy of the observer was affected by PI parameters and motor parameters. The rotor current was estimated by using stator magnetic chain in $\alpha\beta$ coordinate system, its estimation accuracy was directly affected by the estimation error of stator magnetic chain. The existing research results of sensorless technology for the double-fed wind power generation system were all suitable for the operation control of DFIG under ideal power grid conditions. The research on rotor position observer under abnormal power grid conditions has not seen relevant literature.

In this paper, a rotor position observer based on Hysteresis comparator (HC) under unbalanced grid voltage is proposed. This observer calculates the position of the rotor according to the deviation between actual rotor current and the positive sequence component of estimated rotor current. The proposed observer directly estimated the positive sequence component of rotor current by using the positive sequence component of stator voltage and current in the forward synchronous rotating coordinate system dq^P In order to avoid the estimation error caused by stator flux observer, thus the estimation accuracy of rotor current is improved. The simulation results verify the feasibility and correctness of the proposed strategy.

2. Mathematical model of DFIG under the condition of power grid voltage imbalance

The vector equation of voltage and magnetic chain for DFIG under synchronous forward rotation coordinate system dq^P is respectively expressed as

$$\begin{cases} \boldsymbol{u}_{sdq}^P = -R_s \boldsymbol{i}_{sdq}^P + L\dfrac{d\boldsymbol{\psi}_{sdq}^P}{dt} + j\omega_1 \boldsymbol{\psi}_{sdq}^P \\ \boldsymbol{u}_{rdq}^P = -R_r \boldsymbol{i}_{rdq}^P + L\dfrac{d\boldsymbol{\psi}_{rdq}^P}{dt} + j\omega_{slip+} \boldsymbol{\psi}_{rdq}^P \end{cases} \tag{1}$$

$$\begin{cases} \boldsymbol{\psi}_{sdq}^P = -L_s i_{sdq}^P + L_m i_{rdq}^P \\ \boldsymbol{\psi}_{rdq}^P = -L_m i_{sdq}^P + L_r i_{rdq}^P \end{cases} \tag{2}$$

Where

$$\begin{cases} \boldsymbol{u}_{sdq}^P = \boldsymbol{u}_{sdq+}^P + \boldsymbol{u}_{sdq-}^P = \boldsymbol{u}_{sdq+}^P + \boldsymbol{u}_{sdq-}^N e^{-j2\omega_1 t} \\ \boldsymbol{u}_{rdq}^P = \boldsymbol{u}_{rdq+}^P + \boldsymbol{u}_{rdq-}^P = \boldsymbol{u}_{rdq+}^P + \boldsymbol{u}_{rdq-}^N e^{-j2\omega_1 t} \end{cases} \tag{3}$$

$$\begin{cases} \boldsymbol{\psi}_{sdq}^{P} = \boldsymbol{\psi}_{sdq+}^{P} + \boldsymbol{\psi}_{sdq-}^{P} = \boldsymbol{\psi}_{sdq+}^{P} + \boldsymbol{\psi}_{sdq-}^{N} e^{-j2\omega_1 t} \\ \boldsymbol{\psi}_{rdq}^{P} = \boldsymbol{\psi}_{rdq+}^{P} + \boldsymbol{\psi}_{rdq-}^{P} = \boldsymbol{\psi}_{rdq+}^{P} + \boldsymbol{\psi}_{rdq-}^{N} e^{-j2\omega_1 t} \\ \boldsymbol{i}_{sdq}^{P} = \boldsymbol{i}_{sdq+}^{P} + \boldsymbol{i}_{sdq-}^{P} = \boldsymbol{i}_{sdq+}^{P} + \boldsymbol{i}_{sdq-}^{N} e^{-j2\omega_1 t} \\ \boldsymbol{i}_{rdq}^{P} = \boldsymbol{i}_{rdq+}^{P} + \boldsymbol{i}_{rdq-}^{P} = \boldsymbol{i}_{rdq+}^{P} + \boldsymbol{i}_{rdq-}^{N} e^{-j2\omega_1 t} \end{cases} \tag{4}$$

The subscript "+" is the positive sequence component, "-" is the negative sequence component, "s" is the stator, "r" is the rotor, "P" is the positive rotation, and "N" is the reversal. $\boldsymbol{u}_s, \boldsymbol{u}_r, \boldsymbol{i}_s, \boldsymbol{i}_r, \boldsymbol{\psi}_s, \boldsymbol{\psi}_r$ is respectively stator, rotor voltage, current and flux vector. L_m, L_s, L_r is respectively the mutual inductance between the stator and rotor, the equivalent self-inductance of two phase winding in stator and rotor. ω_1 is the synchronous rotation angular frequency of the grid voltage, ω_r is the rotation angular frequency of the rotor, $\omega_{slip+} = \omega_1 - \omega_r$ is the forward rotation differential angular frequency, $\boldsymbol{u}_{rdq-}^{N} e^{-j2\omega_1 t}$, $\boldsymbol{u}_{sdq-}^{N} e^{-j2\omega_1 t}$, $\boldsymbol{\psi}_{sdq-}^{N} e^{-j2\omega_1 t}$, $\boldsymbol{i}_{sdq-}^{N} e^{-j2\omega_1 t}$, $\boldsymbol{i}_{rdq-}^{N} e^{-j2\omega_1 t}$ is respectively the negative sequence twice the frequency component, where $2\omega_1$ is twice the frequency of ω_1, and index $e^{-j2\omega_1 t}$ is the factor of twice the frequency.

Substituting the second row of equation (2) into the second row of equation (1) gets

$$u_{rdq}^{P} = (R_r + j\omega_{slip}\delta L_r)\boldsymbol{i}_{rdq}^{P} + \delta L_r \frac{d\boldsymbol{i}_{rdq}^{P}}{dt} + \frac{L_m}{L_s}(\boldsymbol{u}_{sdq}^{P} + R_s \boldsymbol{i}_{sdq}^{P} - j\omega_r \boldsymbol{\psi}_{sdq}^{P}) \tag{5}$$

Where, $\sigma = 1 - L_m^2 / (L_s L_r)$ is the leakage factor.

The DFIG rotor current is controlled by Proportional integral resonance (PIR) regulator and the rotor current dynamic term $d\boldsymbol{i}_{rdq}^{P} / dt$ in formula (5) is controlled by the output of PIR regulator. Then, the control equation of rotor voltage is as follows

$$u_{rdq}^{P*} = \delta L_r u_{rdq}^{P'} + (R_r + j\omega_s \delta L_r)\boldsymbol{i}_{rdq}^{P} + \frac{L_m}{L_s}(\boldsymbol{u}_{sdq}^{P} + R_s \boldsymbol{i}_{sdq}^{P} - j\omega_r \boldsymbol{\psi}_{sdq}^{P}) = \delta L_r u_{rdq}^{P'} + E_{rdq}^{P} \tag{6}$$

Where, u_{rdq}^{P*} is the reference value of rotor control voltage, E_{rdq}^{P} is the disturbance signal corresponding to the rotor counter electromotive force acting on the PIR controller. $u_{rdq}^{P'}$ is the output of PIR current controller.

3. Rotor position estimation principle based on rotor current

3.1 Estimation model of positive sequence component of rotor current positive synchronous rotating coordinate dq^P

Ignoring the stator resistance R_s, under steady state conditions, the first row in equation (1) is expressed as

$$\boldsymbol{u}_{sdq}^{P} = j\omega_1 \boldsymbol{\psi}_{sdq}^{P} \tag{7}$$

According to equation (2) and (7), equation (8) can be obtained

$$\boldsymbol{i}_{rdq}^{P} = \frac{L_s}{L_m}\boldsymbol{i}_{sdq}^{P} - j\frac{\boldsymbol{u}_{sdq}^{P}}{\omega_1 L_m} \tag{8}$$

Formula (8) is expressed as the positive and negative sequence components

$$\boldsymbol{i}_{rdq+}^{P} + \boldsymbol{i}_{rdq-}^{N} e^{-j2\omega_1 t} = \frac{L_s}{L_m}(\boldsymbol{i}_{sdq+}^{P} + \boldsymbol{i}_{sdq-}^{N} e^{-j2\omega_1 t}) - j\frac{1}{\omega_1 L_m}(\boldsymbol{u}_{sdq+}^{P} + \boldsymbol{u}_{sdq+}^{N} e^{-j2\omega_1 t}) \tag{9}$$

When estimating the rotor current from equation (9), it contains the negative sequence twice frequency component of the rotor current, which can be filtered out by the second order notch filter. The transfer function of the second order notch filter is given as

$$G_{notch} = \frac{s^2 + \omega_0^2}{s^2 + 2\xi\omega_0 s + \omega_0^2} \tag{10}$$

Where $\omega_0 = 2\omega_1 = 200\pi rad/s$ is the cutoff frequency, ξ is the attenuation coefficient ($\xi = 0.707$). The bode diagram of the second order notch filter is shown in Fig.1.

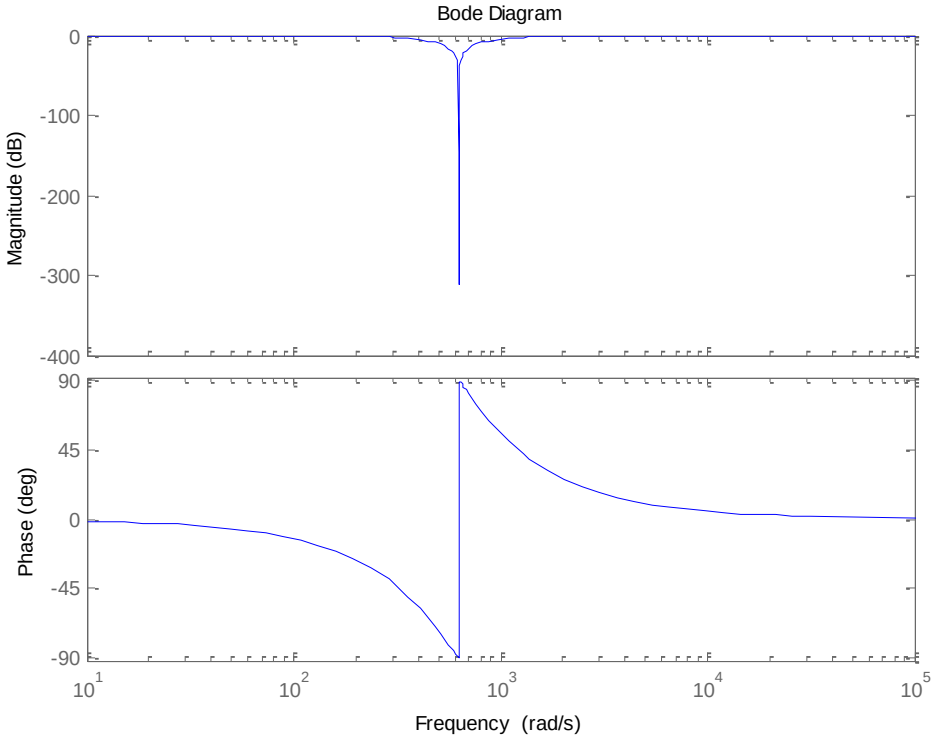

Fig. 1 The bode diagram of the second order notch filter

It can be seen from the Fig.1 that the gain is small near $2\omega_1$ and the double frequency negative sequence component of rotor current can be filtered out. The positive sequence component of rotor current separated by a secondary trap from equation (9) is given as

$$\boldsymbol{i}_{rdq+}^{P} = \frac{L_s}{L_m}\boldsymbol{i}_{sdq+}^{P} - j\frac{\omega_1}{L_m}\boldsymbol{u}_{sdq+}^{P} \tag{11}$$

By placing the forward rotation synchronous rotating coordinate d^p axis is directed to the stator voltage vector $\boldsymbol{u}_{sdq+}^{P}$ can be get

$$\begin{cases} u_{sd+}^{P} = \left|\boldsymbol{u}_{sdq+}^{P}\right| = U_s^P \\ u_{sq+}^{P} = 0 \end{cases} \tag{12}$$

Substitute equation (12) into equation (11) can be obtained

$$\begin{cases} i_{rd+}^{P} = \dfrac{L_s}{L_m} i_{sd+}^{P} \\ i_{rq+}^{P} = -\dfrac{U_s^{P}}{\omega_1 L_m} + \dfrac{L_s}{L_m} i_{sq+}^{P} \end{cases} \tag{13}$$

Equation (13) is the expression of the positive sequence component of rotor current (i_{rdq+}^{p}) obtained by the positive sequence component of stator current (i_{sdq+}^{p}) and stator voltage U_s^p in dq^P coordinate.

Replace i_{rd+}^{p}, i_{rq+}^{p} with $\hat{i}_{rd+}^{p}, \hat{i}_{rq+}^{p}$ the positive sequence component estimation model of rotor current can be obtained

$$\begin{cases} \hat{i}_{rd+}^{P} = \dfrac{L_s}{L_m} i_{sd+}^{P} \\ \hat{i}_{rq+}^{P} = -\dfrac{U_s^{P}}{\omega_1 L_m} + \dfrac{L_s}{L_m} i_{sq+}^{P} \end{cases} \tag{14}$$

The main factor influencing the estimation accuracy in equation (14) is L_s / L_m. The current estimation model as shown in Fig.2.

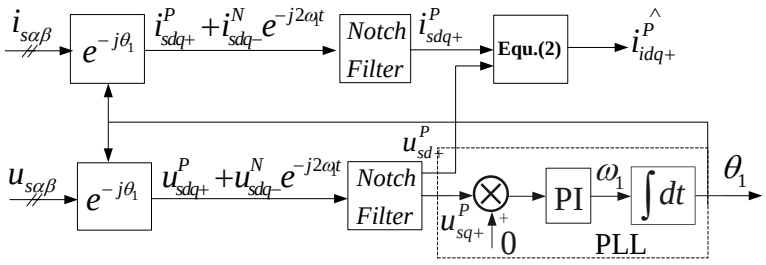

Fig.2 the estimation model of rotor current i_{rdq+}^{p}

The PLL in Fig.2 is the power grid voltage phase-locked loop.

3.2 Build deviation function ε_r

The design core of rotor position observer is to set up rotor position deviation function ε_r, which adjusts rotor position according to ε_r. The construction method is to obtain the rotor current deviation vector by cross multiplying the estimated rotor current vector and the measured rotor current vector in a forward synchronous coordinate system, It is expressed as:

$$\boldsymbol{\varepsilon_r} = \hat{\boldsymbol{i}}_{rdq+}^{P} \times \boldsymbol{i}_{rdq+}^{P} \tag{15}$$

The relationship between $\boldsymbol{\varepsilon_r}$, $\hat{\boldsymbol{i}}^{P}_{rdq+}$ and $\boldsymbol{i}^{P}_{rdq+}$ conforms to the right hand rule.

The module of $\boldsymbol{\varepsilon_r}$ is expressed as

$$\varepsilon_r = \left| \hat{\boldsymbol{i}}^{P}_{rdq+} \times \boldsymbol{i}^{P}_{rda+} \right| = i^{P}_{rq+}\, \hat{i}^{P}_{rd+} - i^{P}_{rd+}\, \hat{i}^{P}_{rq+} = \left| \hat{\boldsymbol{i}}^{P}_{rdq+} \right| \left| \boldsymbol{i}^{P}_{rdq+} \right| \sin\theta_{rerror} \tag{16}$$

Where θ_{rerror} is the deviation angle between the estimated current $\hat{\boldsymbol{i}}^{P}_{rdq+}$ and the actual detection current positive sequence component $\boldsymbol{i}^{P}_{rdq+}$.Because $\hat{\boldsymbol{i}}^{P}_{rdq+}$ contains estimated rotor information $\hat{\theta}_r$ and $\boldsymbol{i}^{P}_{rdq+}$ contains actual rotor position information θ_r ,so θ_{rerror} just is the deviation angle between $\hat{\theta}_r$ and θ_r . $\boldsymbol{\varepsilon_r}$ is the sine function of θ_{rerror} , which represents the actual deviation of rotor position angle, θ_{rerror} can be realized to zero by controlling ε_r to zero, and accurate rotor position and rotor speed can be obtained.

4. Rotor position observer based on HC

The structure of rotor position observer based on HC is shown in Fig.3. The hysteresis comparator is used as the controller in Fig.3. The input of the controller is ε_r and its output is the deviation of the estimated rotor speed $\Delta\hat{\omega}_r$, then the estimated rotor speed $\hat{\omega}_r$ is obtained by integrating $\Delta\hat{\omega}_r$ and the estimated rotor position angle $\hat{\theta}_r$ is obtained by integrating, to the estimated rotor speed $\hat{\omega}_r$ .The principle of HC is shown in Fig.4.

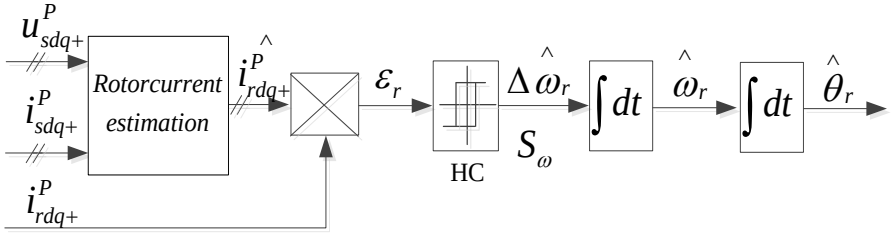

Fig.3 schematic of observer based on the HC controller

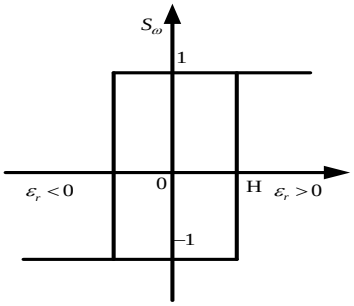

Fig.4 The diagram of hysteresis controller

In Fig.4, H is the loop width of hysteresis controller. In this paper, several different H values are selected for simulation, and the simulation results are analyzed, and the optimal H is zero. When H is zero. The estimated rotor speed $\hat{\omega}_r$ is regulated in real time by HC according to θ_{rerror} , when θ_{rerror} is regulated to approaches zero, to obtain the accurate rotor position θ_r .

5. Simulation and results

In this paper, Matlab simulation technology is used to verify the correctness and feasibility of the proposed HC rotor position observer under the condition of power grid voltage unbalance. During the simulation, the PIR vector control strategy for DFIG under the condition of power grid voltage imbalance in [12] is adopted. The DFIG PIR vector control structure for DFIG based on HC rotor position observer is shown in Fig.5.

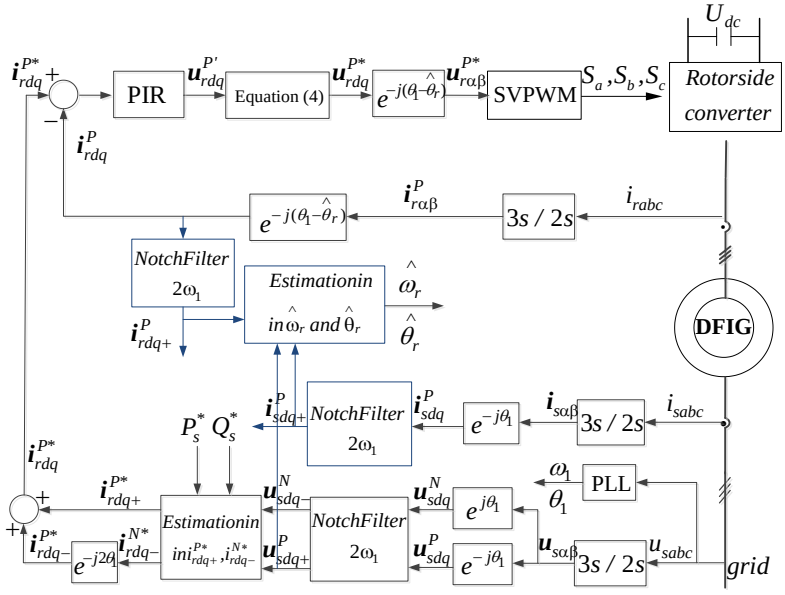

Fig.5 The PIR control strategy of DFIG unbalanced grid voltage conditions

According to Fig.5, the MATLAB simulation model as shown in Fig. 6 is built.

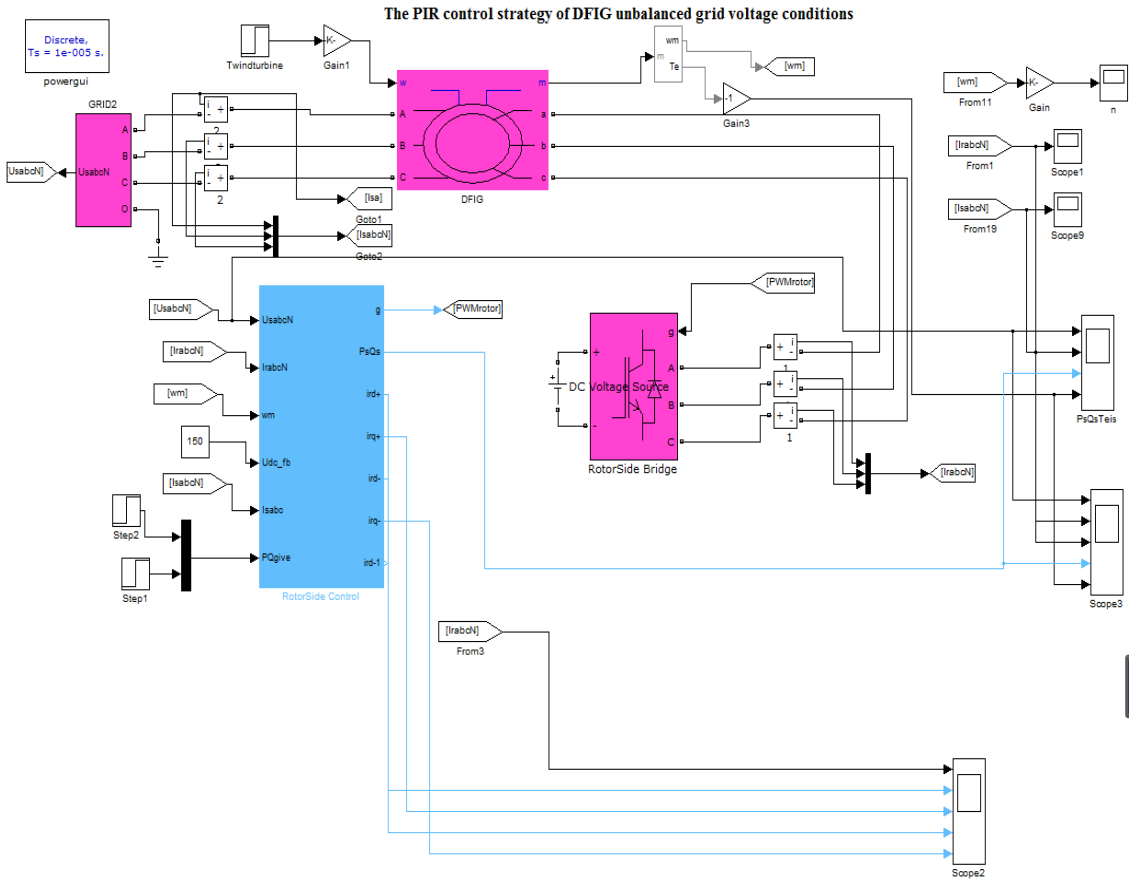

Fig.6 The MATLAB simulation model based on PIR; Control strategy of DFIG unbalanced grid voltage conditions

The connection grid line voltage of DFIG is 270V during simulation. The simulation conditions are as follows: ①the single-phase voltage of the power grid falls is 25%and the failure period is [0.6s 1.2s]. ②the running speed of DFIG wind turbine is 1000r/min. ③The reference values of the output average active and reactive power P_s^* and Q_s^* from stator are respectively 2800W and 0Var. Grid side converter DC bus voltage U_{dc} is 200V. The simulation waveform is shown in Fig.7~Fig.8.

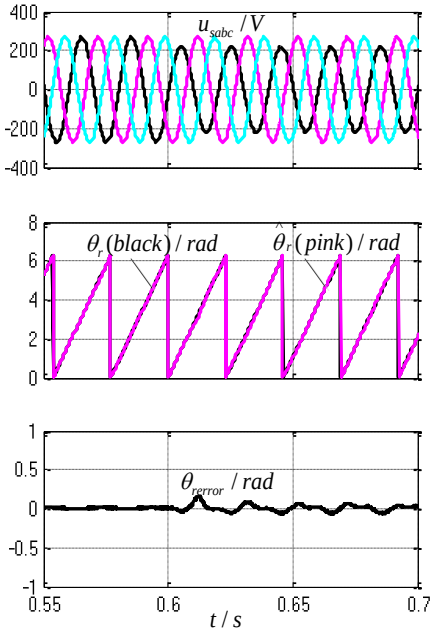

Fig.7 Simulation waveform of the actual and estimated rotor position with 25% of single-phase voltage drop

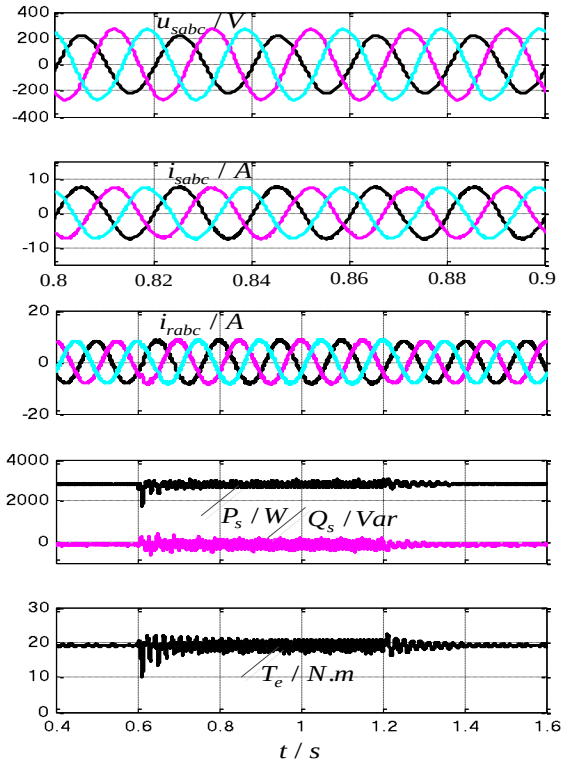

Fig.8 Simulation waveform of DFIG with 25% of single-phase voltage drop

Simulation results show that the proposed rotor position observer based on HC can accurately estimate the rotor position while the power grid fails. The DFIG PIR vector control strategy based on HC rotor position observer has good fault crossing capability.

6. Conclusions

The position observer based on HC are analyzed and discussed under the condition of power grid voltage imbalance in this paper. The simulation results show that the observers can accurately estimate the rotor position under the condition of power grid voltage imbalance.

R E F E R E N C E S

[1]. Wang Peng. Study on Control Strategy of Doubly Fed Wind Generation Frequency Regulation of Power System. Telecom Power Technology, vol. 34, 2017, pp. 66-68.

[2]. Xiao Ya Ping, Xiao Sa, et al. Study on the Operation of ASCF Doubly Fed Wind Power Generator. JOURNAL OF ELECTRIC POWER, vol. 32, 2017, pp. 370-375.

[3]. Sun Liling, Wang Yanjuan. Study on Transient Whole-process and Control Strategy of Stator Fluxin Doubly-fed Induction Generator with Asymmetric Voltage Swell. High Voltage Engineering, vol. 45, 2019, pp. 2160-2166.

[4]. Jiang Huilan, Li Tianpeng, Wu Yuzhang. Integrated strategy for low voltage ride through of doubly-fed induction generator. High Voltage Engineering, vol. 43, 2017, pp. 2062-2068.

[5]. Zhao Meihua, Chen Jun, Ge Kai .Comparative Studies on HC-DPC and SVM P-DPC for Grid-side Converter in Wind Power System Based on DFIG. Proceedings of the CSUEPSA, vol. 27, 2015, pp. 92-97.

[6]. Zhao Mei-Hua, Ruan Yi, Song Wen-Xiang, Ge Kai. Comparison of indirect power control and direct power control for doubly-fed in duction generator. Electric Machines and control, vol. 18, 2014, pp. 68-73.

[7]. Zhou Linyuan, Liu Jinjun, Zhou Sizhan. Demagnetization control for doubly-fed induction generator under balanced grid fault. Power System Technology, vol. 38, 2014, pp. 3424-3430.

[8]. Sun Liling, Wang Yanjuan. Analysis and performance evaluation for transient whole process of improved control strategy for doubly-fed induction generator crossed by high voltage ride through. High Voltage Engineering, vol. 45, 2019, pp. 593-599.

[9]. Zhao Meihua, Zheng Peng, Li Guanglun, Sun Nanhai. Direct power control of doubly-fed induction generator based on hysteresis rotor position detector. Journal of Shao yang University (Natural Science Edition), vol. 14, 2017, pp. 44-49.

[10]. Gao Le, Zhou Youqing, Xu Longya, Guan Bo. Control of speed sensor of double-fed induction motor based on rotor current. Power system automation, vol. 34, 2010, pp. 61-65.

[11]. Kang Zhongjian, Lu Xuezhi, Chen tianli, censorshuwei. Design of rotor position observer for double-fed wind generator with reference to adaptive fuzzy control based on rotor current model. Power system protection and control, 38, 2010, pp. 72-82.

[12]. Hu Jiabing, He Yikang, Xu Lie, et al. Improved control of DFIG system during network unbalance using PI-R current regulators. IEEE transactions On Industrial Electronics, vol. 56, 2009, pp. 439-451.